Plasmon-phonon coupling in graphene

E. H. Hwang, Rajdeep Sensarma, and S. Das Sarma
Condensed Matter Theory Center, Department of Physics, University of Maryland, College Park, Maryland 20742-4111, USA
(Received 20 August 2010; revised manuscript received 18 October 2010; published 3 November 2010)

Collective excitations of coupled electron-phonon systems are calculated for both monolayer and bilayer graphenes, taking into account the nonperturbative Coulomb coupling between electronic excitations in graphene and the substrate longitudinal-optical phonon modes. We find that the plasmon-phonon coupling in monolayer graphene is strong at all densities but in bilayer graphene the coupling is significant only at high densities satisfying the resonant condition $\omega_{pl} \approx \omega_{ph}$. The difference arises from the peculiar screening properties associated with chirality of graphene. Plasmon-phonon coupling explains the measured quasilinear plasmon dispersion in the long-wavelength limit, thus resolving a puzzle in the experimental observations.

DOI: 10.1103/PhysRevB.82.195406 PACS number(s): 81.05.ue, 73.20.Mf, 71.38.−k, 63.22.Rc

I. INTRODUCTION

A plasmon is a collective mode of charge-density oscillation in the free-carrier system, which is present both in classical and quantum plasmas. Studying the collective plasmon excitation in the electron gas has been among the very first theoretical quantum mechanical many-body problems studied in solid-state physics. The collective plasmon modes of monolayer graphene (MLG) have been extensively studied theoretically[1–7] and experimentally.[8–13] Recent discovery of bilayer graphene (BLG) has also led to a number of theoretical descriptions of plasmon modes in BLG.[14,15] Even though the long-wavelength plasmon frequency of MLG is explicitly nonclassical (i.e., the plasmon frequency is necessarily quantum with $\hbar$ appearing manifestly in the long-wavelength plasma frequency[3]), its wave-vector dispersion is given by classical electrodynamics, i.e., $\omega_p(q) \propto \sqrt{q}$. Note that the quadratic band dispersion of BLG makes the leading order long-wavelength plasmon dispersion explicitly classical with the same $\sim\sqrt{q}$ dependence. However, at finite q, away from the long-wavelength limit, there are several corrections to the plasmon dispersion $\omega(q)$ arising from nonlocal finite wave-vector response, finite-temperature thermal corrections, many-body effects, local-field corrections, and other mechanisms relevant to the specific electron system.

Since the plasmon dispersion relation is exactly known at long wavelengths ($q \to 0$) where the f-sum rule arising from particle conservation fixes the plasma frequency, it is surprising that the measured graphene plasmon dispersion in the long-wavelength limit deviates from the classical dispersion ($\omega_q \sim \sqrt{q}$) and shows a rather linear dispersion.[9,12] In a recent experiment,[10] the strongly coupled plasmon-phonon mode dispersion has been measured by the angle-resolved reflection electron energy-loss spectroscopy and it is found that the discrepancy arises from electron-phonon coupling. In epitaxial graphene the substrate (i.e., SiC) is a highly polar material. In general, carriers in polar materials couple with the longitudinal-optical phonons of the system via the long-range Fröhlich interaction. However, the surface optical (SO) phonon is a well-characterized surface property of polar semiconductors, and it is possible that carriers in graphene layer couple to the SO phonons of the underlying substrate lattice via the long-range polar Fröhlich coupling.[16,17] For isotropic media the frequency of SO phonons ω_{SO} is related to the transverse-optical (TO) bulk phonon ω_{TO} as $\omega_{SO}/\omega_{TO} = \sqrt{(\epsilon_0+1)/(\epsilon_\infty+1)}$,[16–18] where ϵ_0 (ϵ_∞) is the static (high-frequency) dielectric constant. Note that the bulk longitudinal optical phonons ω_{LO} and ω_{TO} are connected with the dielectric constants by the Lyddane-Sachs-Teller relation $\omega_{LO}/\omega_{TO} = \sqrt{\epsilon_0/\epsilon_\infty}$.

The electron-phonon coupling is the macroscopic coupling of the electronic collective modes (plasmons) to the optical phonons. The mode-coupling phenomenon, which hybridizes the collective plasmon modes of the electron gas with the optical-phonon modes of the lattice, gives rise to the coupled plasmon-phonon modes (the hybrid modes) which have been extensively studied[19–22] both experimentally and theoretically in bulk and two-dimensional (2D) electron systems. The electron-phonon interaction leads to many-body renormalization of the single-particle free-carrier properties[23,24] and also affects the transport properties.[25,26] A good understanding of electron-phonon coupling is thus important in developing quantitative theories for many different experimental studies in graphene.

In this paper we calculate the coupled plasmon-SO phonon modes of epitaxial graphene (or graphene on a polar substrate such as SiO_2, SiC, or HfO_2). Our most significant finding is that in MLG plasmon-phonon mode-coupling effect is strong at all electronic densities due to the singular behavior in the screening function arising from chirality.[1] By contrast, for BLG, the plasmon-phonon coupling is significant only at high carrier densities. We also find that at low densities, when the coupling is weak and the coupled phononlike mode (gapped mode) lies in the interband electron-hole continuum, the energy of phononlike mode decreases in the long-wavelength limit due to the coupling of the phonon mode to the interband single-particle excitation (SPE), which arises from the enhanced BLG backscattering.[27] However, at high densities, when the plasmon-phonon mode coupling is strong, the phononlike mode frequency increases linearly with wavevector, as in MLG.

The paper is organized as follows. In Sec. II the generalized theory is presented to calculate the total dielectric function of a coupled system within the random-phase approximation (RPA). Section III presents the results of electron-

 ©2010 The American Physical Society

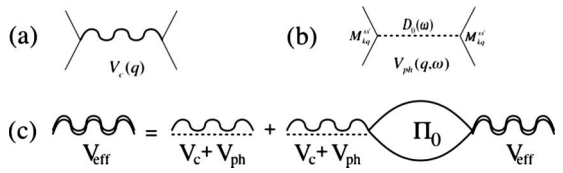

FIG. 1. (a) Electron-electron Coulomb interaction. (b) Phonon mediated electron-electron interaction. (c) Effective dynamical interaction V_{eff} calculated in RPA. Dashed (wiggly) lines represent the SO-phonon mediated (Coulomb) electron-electron interaction V_{ph} (v_c), and the bubble the irreducible polarizability $\Pi_0(q,\omega)$.

phonon couplings in both MLG and BLG. We summarize in Sec. IV with a discussion.

II. THEORY

We first present our model for plasmon-phonon coupling, which consists of a two-dimensional electron gas coupled to dispersionless SO phonons at zero temperature. For MLG, we have a system of Dirac fermions with linear dispersion while BLG have a parabolic dispersion around the Dirac point. Due to the presence of the long-range electron-phonon coupling, electrons interact among themselves through the Coulomb interaction and through virtual-SO-phonon exchange via the Fröhlich interaction. The electron-SO phonon interaction is given by

$$H_{e\text{-}ph} = \sum_{kq} \sum_{ss'} M_{kq}^{ss'} c_{k+qs'}^{\dagger} c_{ks} (b_q + b_{-q}^{\dagger}), \tag{1}$$

where $c_{ks}^{\dagger}$ is the electron ($s=+1$) or hole ($s=-1$) creation operator, $b_q^{\dagger}$ and b_q are creation and destruction operators of surface phonon, and the interaction matrix element $M_s^{ss'}$ is defined by

$$M_{kq}^{ss'} = M_0(q) F_{sk+q}^{\dagger} F_{s'k}, \tag{2}$$

where F_{sk} is the chiral spinor and given by

$$F_{sk} = \frac{1}{\sqrt{2}} \begin{pmatrix} s \\ e^{i\theta_k} \end{pmatrix} \tag{3}$$

with $s=\pm 1$, $\theta_k=\tan^{-1}(k_y/k_x)$ for MLG (Ref. 28) and $\theta_k=2\tan^{-1}(k_y/k_x)$ for BLG.[29,30] We also have

$$[M_0(q)]^2 = \frac{2\pi e^2}{q} e^{-2qd} \frac{\omega_{\mathrm{SO}}}{2} \left[\frac{1}{\epsilon_\infty + 1} - \frac{1}{\epsilon_0 + 1} \right], \tag{4}$$

where d is the separation distance between graphene layer and substrate. The matrix elements of for electron-electron Coulomb interaction shown in Fig. 1(a) is given by

$$v_c^{ss'}(q) = \frac{2\pi q^2}{\epsilon_\infty q} G_{kk'}^{ss'}, \tag{5}$$

where $\mathbf{k}'=\mathbf{k}+\mathbf{q}$ and

$$G_{kk'}^{ss'} = |F_{sk}^{\dagger} F_{s'k+q}|^2 = [1 + ss' \cos(\theta_{kk'})]/2, \tag{6}$$

where $\theta_{kk'}$ is the angle between $\mathbf{k}$ and $\mathbf{k}'$. The SO-phonon mediated electron-electron interaction [Fig. 1(b)] is given by

$$v_{ph}^{ss'}(q,\omega) = [M_0(q)]^2 D_0(\omega) G_{kk'}^{ss'}, \tag{7}$$

which is dependent on both wave vector and frequency. In Eq. (7) $D_0(\omega)$ is the unperturbed SO-phonon propagator and given by

$$D_0(\omega) = \frac{2\omega_{\mathrm{SO}}}{\omega^2 - \omega_{\mathrm{SO}}^2}. \tag{8}$$

The total effective electron-electron interaction is obtained in RPA (Ref. 21) by summing all the bare bubble diagrams [see Fig. 1(c)],

$$v_{eff}(q,\omega) = \frac{v_c(q) + v_{ph}(q,\omega)}{1 - [v_c(q) + v_{ph}(q,\omega)]\Pi_0(q,\omega)} = \frac{v_c(q)}{\epsilon_t(q,\omega)}, \tag{9}$$

where $v_c(q)=2\pi e^2/\epsilon_\infty q$ is the electron-electron Coulomb interaction and $\Pi_0(q,\omega)$ is the complex irreducible polarizability given by the bare bubble diagram

$$\Pi(q,\omega) = -\frac{g_s g_v}{L^2} \sum_{\mathbf{k}ss'} \frac{f_{s\mathbf{k}} - f_{s'\mathbf{k}'}}{\omega + \epsilon_{s\mathbf{k}} - \epsilon_{s'\mathbf{k}'} + i\eta} G_{kk'}^{ss'}, \tag{10}$$

where $\epsilon_{s\mathbf{k}}=sv_F|\mathbf{k}|$, f_{sk} is the Fermi distribution function, $f_{s\mathbf{k}}=[\exp\{\beta(\epsilon_{s\mathbf{k}}-\mu)\}+1]^{-1}$, with $\beta=1/k_BT$ and μ the chemical potential. The irreducible polarizability for the monolayer and the bilayer system is calculated in Refs. 1 and 15, respectively. Then the total dielectric function within RPA contains contributions both from electrons and SO phonons and given by

$$\epsilon_t(q,\omega) = 1 - \frac{2\pi e^2}{\epsilon_\infty q} \Pi_0(q,\omega) + \frac{\alpha e^{-2qd}}{1 - \alpha e^{-2qd} - \omega^2/\omega_{\mathrm{SO}}^2}, \tag{11}$$

where

$$\alpha = \epsilon_\infty \left[\frac{1}{\epsilon_\infty + 1} - \frac{1}{\epsilon_0 + 1} \right]. \tag{12}$$

The collective mode dispersion is given by the zeros of the complex total dielectric function: $\epsilon_t(q,\omega)=0$.

In the case where several surface modes are present, as in SiO_2, carriers couple with each phonon mode through the long-range Fröhlich interaction weighted by the corresponding matrix elements $M_0^{\lambda}(q)$. Then the total electron-electron interaction mediated by phonons is given by

$$v_{ph}(q,\omega) = \sum_{\lambda} [M_0^{\lambda}(q)]^2 D_0^{\lambda}(q,\omega), \tag{13}$$

where D_0^{λ} is the unperturbed phonon propagator for λ-kind phonon. The total dielectric function of a system with several phonons is well approximated by the summing all bare bubble diagrams of the independent contributions. This provides a description of the coupling and interference between phonon modes and plasmon because all these various modes have longitudinal electric fields which cause the mutual coupling. In the following section we provide details of plasmon-phonon coupling effects.

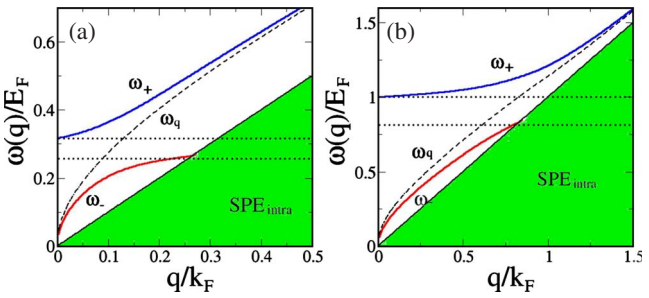

FIG. 2. (Color online) Calculated plasmon-phonon coupled mode $\omega_{\pm}$ dispersions in MLG as a function of the wave vector q for two different densities (a) $n=10^{13}$ cm^{-2} and (b) $n=10^{12}$ cm^{-2}. The plasmon dispersion (ω_q) without the electron-phonon coupling is shown by the dashed line. Two dotted horizontal lines represent the frequencies of the uncoupled SO (top) and TO (bottom) phonon modes, respectively. The colored region represents the intraband single-particle excitation (SPE$_{\text{intra}}$) continuum in which the plasmon is damped by producing electron-hole pairs.

III. RESULTS AND DISCUSSION

A. Monolayer graphene

Let us first focus on the collective modes of MLG. In the long-wavelength limit ($q\to 0$) we get the following coupled $\omega_{\pm}$ collective modes:

$$\omega_{+}(q)=\omega_{\text{SO}}+\frac{\alpha e^{-2qd}}{\omega_{\text{SO}}}\frac{\omega_q^2}{2}, \tag{14a}$$

$$\omega_{-}(q)=(1-\alpha e^{-2qd})\omega_q, \tag{14b}$$

where $\omega_q^2=2e^2E_Fq/\epsilon_{\infty}$ (E_F=Fermi energy) is the plasmon mode dispersion of an uncoupled system in the long-wavelength limit. As $q\to 0$ the phononlike mode ω_+ is located above ω_{SO}. It increases linearly with q and with a slope which is proportional to the Fermi energy. This linear plasmon dispersion as $q\to 0$ is not related to the finite wave-vector quasilinear dispersion observed in experiments.[9,12] However, our prediction of Eq. (14a) can be observed at low densities where the coupling is weak. The plasmonlike ω_- is slightly lower in energy than the corresponding uncoupled monolayer graphene plasmon mode, ω_q.

In Fig. 2 we show the calculated coupled plasmon-phonon collective modes in MLG for two different densities. The following parameters are used throughout this paper:[31] $\omega_{\text{TO}}=95.0$ meV, $\omega_{\text{SO}}=116.7$ meV, $\epsilon_{\infty}=6.4$, $\epsilon_0=10.0$, and $d=5$ Å. As shown in Fig. 2 the mode coupling in MLG is strong for all electron densities. In ordinary 2D systems or three-dimensional systems the plasmon-phonon mode coupling is only significant at densities satisfying the resonant condition $\omega_q\approx\omega_{\text{SO}}$. However, in MLG the plasmon mode exists for all wave vectors due to the singular behavior in the polarizability, which leads to strong plasmon-phonon coupling. Since the singular behavior of the polarizability arise from the suppression of the back scattering due to the chirality of MLG the strong plasmon-phonon coupling is a direct consequence of its unique chiral property of MLG. Note that the plasmonlike mode ω_- in Fig. 2 vanishes at a finite critical wave vector, $q_c\simeq\omega_{\text{SO}}(1-\alpha)/v_F$, and for $q>q_c$ we find only the phononlike mode (ω_+) which approaches ω_q for large q. Figure 2(a) also shows that the phononlike mode ω_+ increases linearly at finite q, which is observed in the recent experiments.[9,12] This quasilinear dispersion at finite q occurs at high densities for $E_F\gg\omega_{\text{SO}}$ and arises from corrections such as finite wave-vector nonlocal effects and many-body effects[1,10] in addition to the plasmon-phonon coupling considered in the current work. We note that the experimentally observed quasilinear dispersion[9,12] is not related the coupling of surface mode to the bulk plasmon mode found in metals[32] because the substrates in experiments are insulators and the coupling to the bulk plasmon mode does not occur.

The dynamical structure factor, $S(q,\omega)$, which gives the spectral weight of the collective modes, is proportional to the imaginary part of the inverse dielectric function (loss function) and given by

$$S(q,\omega)=-\frac{1}{n_0v_c(q)}\text{Im}\left[\frac{1}{\epsilon_t(q,\omega)}\right]. \tag{15}$$

For a true collective mode with zero Landau damping both $\text{Im}[\epsilon_t(q,\omega)]$ and $\text{Re}[\epsilon_t(q,\omega)]$ vanish, and the inverse dielectric function becomes a delta function with weight

$$W(q)=\pi\left[\frac{\partial}{\partial\omega}\text{Re}\ \epsilon_t(q,\omega)|_{\omega=\omega_i(q)}\right]^{-1}, \tag{16}$$

where $\omega_i(q)$ is the collective mode frequency at wave vector q. In the long-wavelength limit the weight of plasmonlike mode can be calculated as

$$W(q)|_{\omega_-}=\frac{\pi}{2}(1-\alpha)^{3/2}\omega_q \tag{17}$$

and the weight of phononlike mode as

$$W(q)|_{\omega_+}=\pi\alpha\omega_{\text{SO}}/2. \tag{18}$$

The spectral weight of ω_- mode vanishes as $\sqrt{q}$ in the long-wavelength limit but the weight of ω_+ mode is finite. Thus in the long-wavelength limit all spectral weight is carried by the phononlike mode. In Fig. 3 the calculated loss function $-\text{Im}[1/\epsilon(q,\omega)]$ is shown in (q,ω) space for two different densities (a) $n=10^{13}$ cm^{-2} and (b) $n=10^{12}$ cm^{-2}. In the long-wavelength limit the phononlike mode has most of the weight. In the intermediate wave-vector range, however, the plasmonlike mode becomes stronger. The weight of the ω_- mode vanishes again when the plasmonlike mode merges with the electron-hole continuum at a critical wave vector and ω_- mode becomes overdamped by Landau damping.

B. Bilayer graphene

Let us now turn our attention to BLG. Just like MLG, we again get two hybridized plasmon-phonon modes, one (ω_-) having a $\sim\sqrt{q}$ dispersion and the other (ω_+) exhibiting a gap equal to the SO phonon frequency (ω_{SO}) in the long-wavelength limit. The ω_- mode has the same dispersion as in MLG, $\omega_-(q)=(1-\alpha e^{-2qd})\omega_q$, which lies in the gap between the intraband and interband continua and has a spectral weight which goes as $\sim\sqrt{q}$. Thus, in the long-wavelength

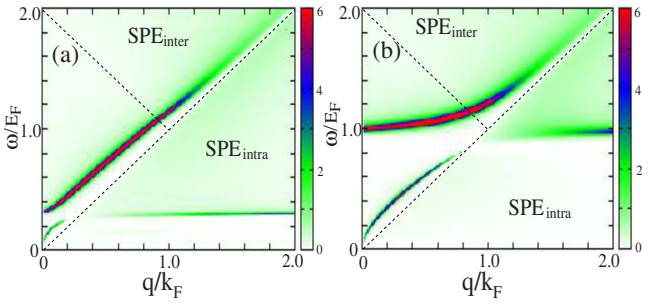

FIG. 3. (Color online) The density plots of energy-loss function $(-\mathrm{Im}[1/\epsilon(q,\omega)])$ of MLG in (q,ω) space for two different densities (a) $n=10^{13}$ cm^{-2} and (b) $n=10^{12}$ cm^{-2}. Note that the ω_+ mode of the high-density result carries most spectral weight and its dispersion is almost linear, which is observed in the recent experiment (Ref. 9). We use a phenomenological damping of $0.1E_F$ in these results.

limit, all the oscillator strength lies in the gapped mode ω_+.

However, there are two main differences from MLG, i.e., the quadratic energy dispersion and the enhanced backscattering due to chirality in BLG,[27] which lead to nontrivial differences in the collective mode spectrum. These two effects lead to very different behavior in the low- and high-density limits. To illustrate these effects, we plot the collective mode spectrum of bilayer graphene at two different densities, (a) $n=10^{13}$ cm^{-2} (high density, $E_F>\omega_{\mathrm{SO}}$) and (b) $n=10^{12}$ cm^{-2} (low density, $E_F<\omega_{\mathrm{SO}}$) in Fig. 4. Here, ω_q is the uncoupled plasmon frequency and the shaded regions represent the intraband and interband particle-hole continua. The corresponding loss functions are plotted in Fig. 5.

In the high-density limit where $w_q\sim\omega_{\mathrm{SO}}$, there is a strong plasmon-phonon coupling as evidenced by the deviations of ω_+ from ω_{SO} and of ω_- from ω_q, which gives rise to the gapped mode ω_+ having a linear dispersion with a positive slope in the low q limit. At larger q values, it approaches the uncoupled plasmon dispersion, as seen in Fig. 4(a). The ω_- mode merges into the continuum at a critical wave vector q_c, which is much smaller than that of the uncoupled mode indicating strong electron-phonon coupling. Furthermore, as seen from Fig. 5(a), the phononlike mode ω_+ carries a much larger spectral weight than ω_-.

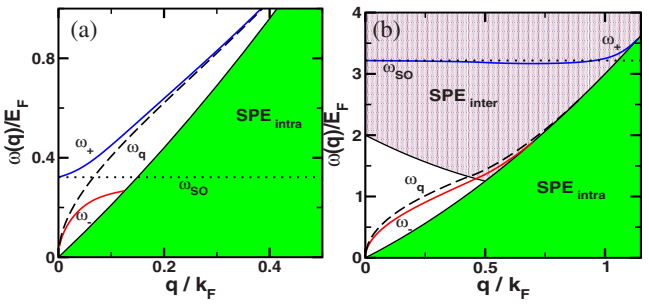

FIG. 4. (Color online) Calculated plasmon-phonon coupled mode $\omega_\pm$ dispersions in bilayer graphene as a function of the wave vector q for two different densities (a) $n=10^{13}$ cm^{-2} and (b) $n=10^{12}$ cm^{-2}. The plasmon dispersion (ω_q) without the electron-phonon coupling is shown by the dashed line. The dotted horizontal line represent the frequency of the uncoupled SO phonon mode.

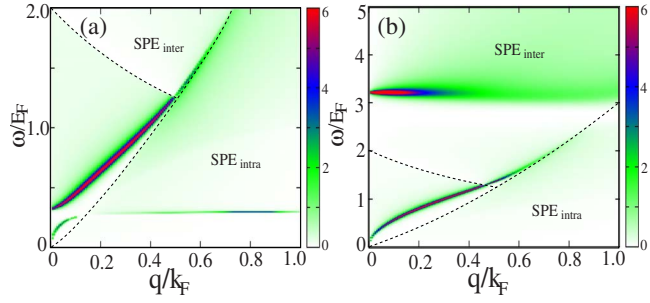

FIG. 5. (Color online) The density plots of energy-loss function $(-\mathrm{Im}[1/\epsilon(q,\omega)])$ of bilayer graphene in (q,ω) space for two different densities (a) $n=10^{13}$ cm^{-2} and (b) $n=10^{12}$ cm^{-2}.

In the low-density limit where $\omega_q<\omega_{\mathrm{SO}}$, the plasmon-phonon coupling is weak and the gapped mode ω_+ is barely affected by the coupling. In addition, the mode energy decreases linearly in the long-wavelength limit, as seen in Fig. 4(b). The small negative slope is a consequence of the coupling of the phonon mode to the interband SPE (Ref. 15) arising from the enhanced backscattering in the system and is a distinct difference between the MLG and BLG. Note that when the SO phonon mode is pushed into the interband electron-hole continuum, the coupled ω_+ mode is always Landau damped due to the presence of the interband continuum and carries little spectral weight beyond a very small range of low q values. The deviation of the plasmonlike mode ω_- from the uncoupled dispersion is much smaller than in the high-density limit, further showing that the plasmon-phonon coupling is weak in this limit. From Fig. 5(b), we find that beyond a small range of low q values, the plasmonlike mode carries much more spectral weight than the phononlike mode and hence, at low densities, the plasmon mode should be easier to detect in BLG.

IV. SUMMARY

In summary, we have calculated the dispersion and the spectral weight of the coupled plasmon-phonon mode of 2D graphene. We find that the mode-coupling effect is strong in monolayer graphene at all densities in contrast to the corresponding bilayer graphene, where the coupling is only significant at high densities. The role of substrate phonons could be easily discerned by looking at the plasmon dispersion, showing conclusively that the substrate phonons would show up directly in the graphene plasmon dispersion. Since the carriers in graphene are strongly coupled to the surface optical phonon of a polar substrate it is important to include electron-SO phonon interaction in the many-body renormalization of the single-particle properties, which has been only considered in the presence of electron-electron interaction[33] and electron-graphene phonon interaction.[23,24,34] The issue of substrate phonons in graphene is also important for experimental transport properties.[26] Finally, we emphasize a definitive prediction of our theory would be a rather variable experimental plasmon dispersion for graphene on different substrates since the plasmon-phonon coupling would depend

on the details of the substrate phonons—in particular, there would be no plasmon-phonon coupling for suspended graphene whereas the coupling effects predicted in this work will be very strong for graphene on SiC or HfO_2.

ACKNOWLEDGMENTS

This work is supported by ONR-MURI and SWAN-NRI.

[1] E. H. Hwang and S. Das Sarma, Phys. Rev. B **75**, 205418 (2007).
[2] E. H. Hwang and S. Das Sarma, Phys. Rev. B **80**, 205405 (2009).
[3] S. Das Sarma and E. H. Hwang, Phys. Rev. Lett. **102**, 206412 (2009).
[4] B. Wunsch, T. Stauber, F. Sols, and F. Guinea, New J. Phys. **8**, 318 (2006).
[5] X.-F. Wang and T. Chakraborty, Phys. Rev. B **75**, 033408 (2007).
[6] O. Vafek, Phys. Rev. Lett. **97**, 266406 (2006).
[7] K. F. Allison and Z. L. Miskovic, Nanotechnology **21**, 134017 (2010).
[8] C. Kramberger, R. Hambach, C. Giorgetti, M. H. Rümmeli, M. Knupfer, J. Fink, B. Büchner, L. Reining, E. Einarsson, S. Maruyama, F. Sottile, K. Hannewald, V. Olevano, A. G. Marinopoulos, and T. Pichler, Phys. Rev. Lett. **100**, 196803 (2008).
[9] Y. Liu, R. F. Willis, K. V. Emtsev, and T. Seyller, Phys. Rev. B **78**, 201403 (2008).
[10] Y. Liu and R. F. Willis, Phys. Rev. B **81**, 081406 (2010).
[11] R. Koch, T. Seyller, and J. Schaefer, arXiv:1008.1130 (unpublished).
[12] T. Langer, J. Baringhaus, H. Pfnür, H. W. Schumacher, and C. Tegenkamp, New J. Phys. **12**, 033017 (2010); C. Tegenkamp, H. Pfnuer, T. Langer, J. Baringhaus, and H. Schumacher, arXiv:1008.1013 (unpublished).
[13] J. Lu, K. P. Loh, H. Huang, W. Chen, and A. T. S. Wee, Phys. Rev. B **80**, 113410 (2009).
[14] G. Borghi, M. Polini, R. Asgari, and A. H. MacDonald, Phys. Rev. B **80**, 241402 (2009).
[15] R. Sensarma, E. H. Hwang, and S. Das Sarma, arXiv:1006.3078 (unpublished).
[16] R. Fuchs and K. L. Kliewer, Phys. Rev. **140**, A2076 (1965).
[17] S. Q. Wang and G. D. Mahan, Phys. Rev. B **6**, 4517 (1972).
[18] L. H. Dubois and G. P. Schwartz, Phys. Rev. B **26**, 794 (1982).
[19] G. Abstreiter, M. Cardona, and A. Pinczuk, in *Light Scattering in Solids IV*, edited by M. Cardona and G. Gntherodt (Springer-Verlag, New York, 1984).
[20] R. Matz and H. Lüth, Phys. Rev. Lett. **46**, 500 (1981).
[21] R. Jalabert and S. Das Sarma, Phys. Rev. B **40**, 9723 (1989).
[22] E. H. Hwang and S. Das Sarma, Phys. Rev. B **52**, R8668 (1995).
[23] W.-K. Tse, E. H. Hwang, and S. Das Sarma, Appl. Phys. Lett. **93**, 023128 (2008).
[24] C.-H. Park, F. Giustino, C. D. Spataru, M. L. Cohen, and S. G. Louie, Phys. Rev. Lett. **102**, 076803 (2009).
[25] S. Fratini and F. Guinea, Phys. Rev. B **77**, 195415 (2008).
[26] J. H. Chen, C. Jang, S. D. Xiao, M. Ishigami, and M. S. Fuhrer, Nat. Nanotechnol. **3**, 206 (2008); K. Zou, X. Hong, D. Keefer, and J. Zhu, Phys. Rev. Lett. **105**, 126601 (2010).
[27] E. H. Hwang and S. Das Sarma, Phys. Rev. Lett. **101**, 156802 (2008).
[28] T. Ando, J. Phys. Soc. Jpn. **75**, 074716 (2006).
[29] M. Koshino and T. Ando, Phys. Rev. B **73**, 245403 (2006).
[30] E. McCann and V. I. Fal'ko, Phys. Rev. Lett. **96**, 086805 (2006).
[31] H. Nienhaus, T. U. Kampen, and W. Mönch, Surf. Sci. **324**, L328 (1995).
[32] B. Diaconescu, K. Pohl, L. Vattuone, L. Savio, P. Hofmann, V. M. Silkin, J. M. Pitarke, E. V. Chulkov, P. M. Echenique, D. Farias, and M. Rocca, Nature (London) **448**, 57 (2007).
[33] M. Polini, R. Asgari, G. Borghi, Y. Barlas, T. Pereg-Barnea, and A. H. MacDonald, Phys. Rev. B **77**, 081411 (2008); E. H. Hwang and S. Das Sarma, *ibid.* **77**, 081412 (2008).
[34] V. W. Brar, S. Wickenburg, M. Panlasigui, C. H. Park, T. O. Wehling, Y. Zhang, R. Decker, C. Girit, A. V. Balatsky, S. G. Louie, A. Zettl, and M. F. Crommie, Phys. Rev. Lett. **104**, 036805 (2010).